Measurement 234 (2024) 114865

Contents lists available at ScienceDirect

Measurement

journal homepage: www.elsevier.com/locate/measurement

Automated thickness measurement system for nuclear fuel plates: A metrological study

Marcelo Kobayoshi [a,*], Ricardo Mendes Leal Neto [a], Elita Fontenele Urano de Carvalho [a], Michelangelo Durazzo [a]

[a] Nuclear and Energy Research Institute, IPEN-CNEN/SP, São Paulo, SP, Brazil

ARTICLE INFO

Keywords:
Metrological reliability
Measurement uncertainty
Measurement capability index
Fuel plate
Nuclear fuel

ABSTRACT

Thickness measurements of nuclear fuel plates manufactured at the Nuclear Fuel Center of the Nuclear and Energy Research Institute (IPEN-CNEN/SP) are currently performed using manual external U-shaped frame micrometers with non-rotating spindles and beveled measurement anvils. Results are then manually recorded on dedicated forms. To improve the efficiency and the metrological reliability of the process, a novel thickness measurement system for nuclear fuel plates was developed. This work presents a comprehensive metrological study of the newly designed measurement system, achieved through the construction of a new apparatus with automated mechanisms for synchronized movement, data capture, transcription, and processing. The study results demonstrate the metrological adequacy of the developed system and underscore the importance of the design and structural quality of the measurement equipment. Consequently, the metrological reliability of the results in the dimensional control of nuclear fuel plates is confirmed.

1. Introduction

Located at the University of São Paulo, Brazil, the Institute of Energy and Nuclear Research (IPEN-CNEN/SP) currently operates two nuclear research reactors. The first reactor, called IEA-R1, is an open pool-type reactor that uses light water for shielding, moderation, and cooling. Its core is made up of a 5×5 array, consisting of 20 fuel elements, 4 control elements, and a central irradiation device [1]. The second reactor, named IPEN-MB-01, is a zero-power nuclear reactor designed to operate at a maximum power of 100 W. Its core is composed of 19 plate-type fuel elements, which simulate the neutron physics of the future Brazilian Multipurpose Reactor (RMB), planned for construction in Brazil [2,3]. Both reactors contain fuel elements that are made up of flat and parallel fuel plates, mechanically mounted in two aluminum side supports with grooves [1].

IPEN-CNEN/SP is responsible for the manufacture of these elements, including their fuel plates, which are made using the traditional "picture-frame" technique [4–6]. The fuel plates are manufactured by rolling and contain the fissile meat completely isolated from the reactor environment, as illustrated in Fig. 1. The meat is produced using conventional powder metallurgy techniques and is composed of a dispersion of U_3Si_2 particles in a matrix of aluminum. Details of the fuel plate manufacturing process at IPEN-CNEN/SP are available in the literature [7].

The total thickness tolerance of the plate influences the minimum thickness of the cladding that protects the fuel meat from the reactor environment, and therefore, must be limited. Any release of fission products into the reactor coolant caused by the exposure of the fuel plate meat leads to operational and safety issues. Additionally, the thickness of the fuel plate influences the dimensions of the fuel element cooling channel, whose control is important from the perspective of the thermal–hydraulic performance of the fuel element. If there are stringent requirements for channel spacing, these cannot be achieved if tolerances for fuel plate thickness are too large. Therefore, the thickness of fuel plates must be carefully controlled and known [8].

Each type of fuel element is specified and produced according to the characteristics of the reactor in which it will be used. In addition to meeting manufacturing requirements, it must comply with inspection requirements and acceptance criteria [4]. As mentioned, fuel plates are currently manufactured at IPEN-CNEN/SP, which constitute the fuel elements of the IEA-R1 and IPEN-MB-01 research reactors. Thickness specifications are differentiated according to the reactors where they

* Corresponding author at: Av. Prof. Lineu Prestes, 2242, Cidade Universitária, CEP 05508-000 São Paulo, SP, Brasil.
E-mail addresses: marcelo.k@ipen.br (M. Kobayoshi), lealneto@ipen.br (R.M. Leal Neto), elitaucf@ipen.br (E.F. Urano de Carvalho), mdurazzo@ipen.br (M. Durazzo).

https://doi.org/10.1016/j.measurement.2024.114865
Received 7 February 2024; Received in revised form 2 May 2024; Accepted 6 May 2024
Available online 7 May 2024

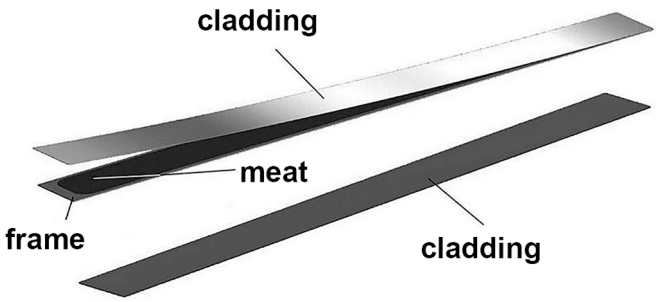

Fig. 1. Exploded view of the fuel plate after rolling.

will be applied and their mounting position in the fuel element.

At IPEN-CNEN/SP, the final manufacturing dimensions of fuel plates are determined by measuring the length, width, and thickness [4], these controls being duly carried out and documented in accordance with standardized and previously authorized operational procedures and work instructions.

Specifically, regarding the control of the thickness of fuel plates, the current work instructions determine that the measurement must be carried out at 21 pre-established points identified through coordinates relative to the reference faces of the plate (Fig. 2). To conduct thickness measurements, manual external U-shaped frame micrometers with non-rotating spindles and beveled measurement anvils are used (Fig. 3) [7], with the positioning of the instrument anvils, in relation to the plate coordinates, assisted by means of a template made of acrylic (polymethyl methacrylate). After readings on the instrument scales, the values of the thickness measurement results are recorded manually, by the operators, on standardized forms.

It has been confirmed that the average time for a trained operator to complete a measurement cycle at the 21 predetermined points on the fuel plate is 20 min, including the time needed for manual recording on standardized forms. The use of external micrometers to measure the thickness of fuel plates is a widely accepted method [9], although it is acknowledged that this process can be time-consuming and heavily reliant on the operator's expertise.

The analysis of data obtained from these measurements follows the guidelines outlined in the document JCGM 100:2008 (Evaluation of Measurement Data – Guide to the Expression of Uncertainty in Measurement), internationally known as GUM [10,11]. This methodology involves conducting 3 measurement cycles on each fuel plate, resulting in 3 data points for each of the 21 measured points, totaling to 63 data points collected for each fuel plate. By adopting this approach, it ensures accuracy and consistency in the measurement process.

The implementation of this methodology, which incorporates the measurement uncertainty approach as a parameter to express measurement variability, has had a significant impact on both operational procedures and decision-making processes. This is especially evident in the evaluation of whether or not to accept a fuel plate, as it now requires

Fig. 3. Manual external U-shaped frame micrometers used for measuring the fuel plate thickness at IPEN-CNEN/SP.

a probabilistic analysis. This approach is in accordance with the guidelines set by the ISO 14253–1:2017, UKAS LAB-48:2022, and ASME B89.7.3.1:2001 standards [12–14] and the EUROLAB Technical Report No.1/2017 [15], which provide clear rules for verifying the conformity of a product characteristic, taking into account the uncertainty of the measurement results. The relationship between the conformity acceptance interval A_I, measurement uncertainty U_p, and specification interval S_I (thickness tolerance requirements) is further illustrated in Fig. 4. This allows for a more accurate and comprehensive assessment of product quality, ensuring that any variations or uncertainties in measurement are taken into consideration.

In the same sense, the guiding document JCGM 106:2012 [16] presents a comprehensive standardization of procedures to be used to verify the conformity of items with specified requirements and addresses in a very complete way the use of measurement results to decide, by acceptance or rejection, of an item of interest to meet a specified requirement. The document proposes a parameter that characterizes the quality of the measurement, in relation to a requirement, specified by a specification interval, which is called measurement capability index C_m

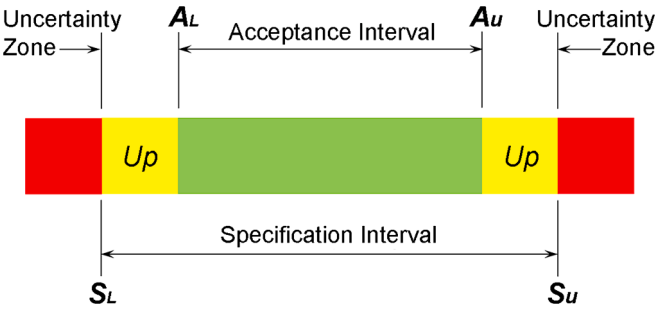

Fig. 4. Conformity acceptance limits.

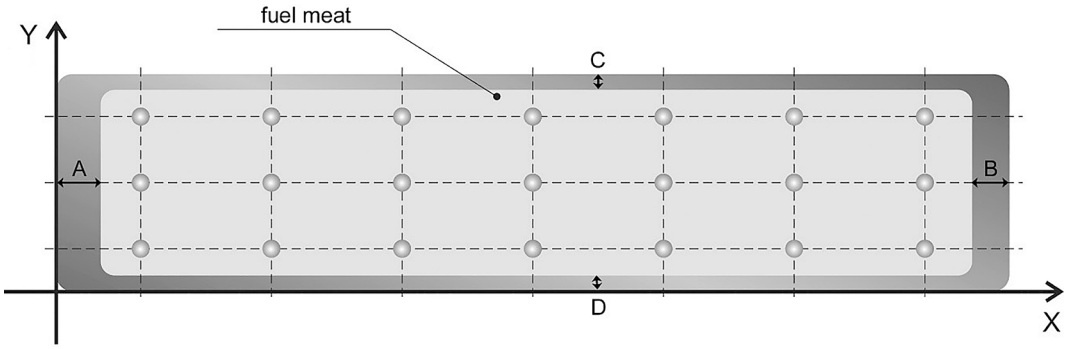

Fig. 2. Typical pre-established point scheme for measuring the fuel plate thickness.

and defined by equation (01):

$$C_m = \frac{S_U - S_L}{4u_c} = \frac{S_I}{2U_{95}} \quad (01)$$

where:

S_U = Upper specification limit.
S_L = Lower specification limit.
u_c = Combined measurement uncertainty.
S_I = Specification interval (tolerance requirements).
U_{95} = Expanded uncertainty ($k = 2.0$).

The JCGM 106:2012 [16] also highlights that, when developing this equation, it was assumed that the distribution of values obtained presents a probability density function represented by a Gaussian curve, where the probability of coverage for this interval is approximately 95 %.

Based on these concepts, and considering the operational safety issues of reactors, IPEN-CNEN/SP adopted in its decision rules for fuel plate thickness the conservative acceptance criterion [17], also known as strict acceptance [14] and as positive compliance for acceptance [15]. Therefore, the acceptance interval of the plates A_I must always be equal to the specification interval S_I minus twice the expanded uncertainty value of the measurement carried out U_p, as shown in Fig. 4.

However, considering the costs involved in the fuel plate manufacturing and control processes, IPEN-CNEN/SP defined in its operational procedures that the expanded uncertainties U_{95} obtained in the measurement results should always be equal or less than 10 % of the specification interval S_I for the thickness of the fuel plates, thus obtaining an adequate technical-financial balance between the plate specifications and the quality of the measurements.

The mathematical analysis of equation (01) shows that the measurement capability indices C_m are directly related to the values of the combined measurement uncertainty u_c obtained in the measurement results, so we have that:

$$C_m \geq 5 \rightarrow u_c \leq \frac{S_I}{20} \quad (02)$$

Using the same reasoning, and assuming that the distribution of the measurement values presents a probability density function represented by a Gaussian curve, where the probability of coverage for such an interval is approximately 95 %, it can be concluded that:

$$C_m \geq 5 \rightarrow U_{95} \leq \frac{S_I}{10} \quad (03)$$

In other words, considering the limit of 10 % of the value of specification interval S_I of the fuel plate thickness for the expanded uncertainties U_{95} obtained in the measurement results, the lowest permissible value for the measurement capability index C_m is equal to 5.

It is important to highlight that, in the specifications of the fuel plates manufactured at IPEN-CNEN/SP, there is a significant difference found in the thickness specification interval S_I, depending on the reactors. For the IEA-R1 fuel plate, the interval is 0.15 mm, whereas for the IPEN/MB-01 fuel plate, this interval is 0.04 mm. A reduction in the thickness specification interval S_I of approximately 73.3 %.

The expanded uncertainties U_{95} arising from the current measurement method adopted at IPEN using micrometers reach the value of ± 0.015 mm. Therefore, considering the acceptance criteria determined by IPEN-CNEN/SP, it is observed that the uncertainty value found is acceptable for measuring the thickness of the plates for use in the IEA-R1 reactor. However, this same value of measurement uncertainty is totally inadequate for the specification interval S_I in the plates manufactured for the IPEN/MB-01 reactor, according to the summary presented in Table 1.

Based on the literature review, it was observed that, although there are several research projects aimed at the control, measurement, and analysis of nuclear fuels, most of these are not directly related to the control processes for the manufacture of fuel plates, but are developed for verifying and measuring dimensional variations and other functional characteristics occurring in fuel elements during or after their application in the nuclear reactor [18–22].

Table 1
Thickness specification for the external micrometer measurement of the fuel plates. Specification interval S_I, expanded uncertainty U_{95}, and measurement capability index C_m.

Reactor	Specification interval (thickness tolerance) S_I (μm)	2 x Expanded Uncertainty $2 \times U_{95}$ (μm)	Measurement Capability Index C_m
IEA-R1	(1.620–1.470) = 150	(2 × 15) = 30	5.00
IPEN-MB-01	(1.370–1.330) = 40	(2 × 15) = 30	1.33

From the above considerations, the main motivation of this work is to enhance the metrological reliability of the results produced and improve the speed of the measurement procedure. This led to the development of a measurement system, implemented thorough the construction of a novel apparatus equipped with photoelectric transmission encoders for automated measurement of fuel plates.

The new apparatus comprises automated mechanisms for movement, data capture, transcription, and data processing. Thus, the main purpose of this work is to present the metrological study conducted to assess the reliability of this new measurement system.

2. Method

2.1. Measurement apparatus

The measurement system was developed to allow automated measurement of the thickness of fuel plates, operating with minimal human interference both in performing the measurement and in the acquisition, transcription and mathematical processing of the data.

The equipment consists of an automated movement system, using displacement motors controlled by a programmable logic controller and a data acquisition and transmission system, composed of measurement sensors based on optical linear encoders, a communication module and a switch.

Other components integrated into the system include fiber optic tangential detectors for plate referencing, linear displacement transducers for determining coordinate systems in the measurement plane and a processing system for mathematical treatment and analysis of results. An overview of the equipment is shown in Fig. 5.

Thickness measurement of fuel plate (1) is performed differentially

Fig. 5. General view of the equipment for automated measurement of nuclear fuel plates.

using two opposing measurement sensors. These sensors are mounted on sensor height adjustment supports, which are in turn fixed to the single-body structure known as the measurement arch (3).

The measurement arc is supported by the X-axis (4) transporters, and its movement is driven by a stepper motor. The translation coordinates of the measurement arc are captured by the X-axis linear transducer. This assembly, in turn, is mounted on the Y-axis (5) transporters, and its displacement is driven by a servo motor. The translation coordinates of the measurement arc are captured by the Y-axis linear transducer.

The entire assembly is supported by a steel structural base (6), which is supported on the ground by vibration dampers. The support beams of the positioners are also fixed to this same structural base, where the components that make up the fuel plate measurement stand are located. Fig. 6 shows the main components identified by the numbers.

In the measurement system integration, the communication between the programmable logic controller (PLC) with the human–machine interface (HMI) and the processing system (Desktop) was implemented through a commutator device (Switch) by local area network (Ethernet).

Data communication between the optical linear encoders (OLE) sensors and the PLC was carried out through the integrated indication and communication component (Module) using a serial communication transmission protocol (RS-232C).

The reception data in the PLC of the X and Y coordinates from the linear displacement scales (transducers) and signals from the optical fiber sensor (OFS) was made possible through integrated digital circuits using bipolar junction transistors and a transistor-to-transistor logic (TTL) class.

In the same way, the TTL logic class was used to send the PLC signals to the drivers for the X and Y axis displacement motors and to send the signals to the solenoid valves (Controller) that command the flow of compressed air to the pneumatic cylinders of the OLE sensors.

The PLC programming was developed in a graphical programming language based on the circuit diagrams (Ladder) aided by a standard model library (STL). The data reception, processing and modeling algorithm and the elaboration of the mathematical model to carry out the calculation of the uncertainty analysis of the measurement results, as well as the generation of surface response curves were programmed using the Microsoft spreadsheet program (Excel) with the complement in visual basic for applications (VBA). Fig. 7 shows the system schematic diagram.

During the design and construction of the equipment, various structural factors were considered, such as reference systems, rigidity of the assembly, degrees of freedom of the plate under measurement, contact methods, fixation systems, and influencing factors in the system, parallax errors, Abbe errors, and potential angular deviations.

Upon completion of the manufacturing, integration, and installation stages of the equipment in the metrology laboratory of IPEN-CNEN/SP, functional tests were initiated. These tests involved executing actuation commands and verifying the movement responses, as well as validating the transmission of signals by assessing the reliability and integrity of data throughout the network.

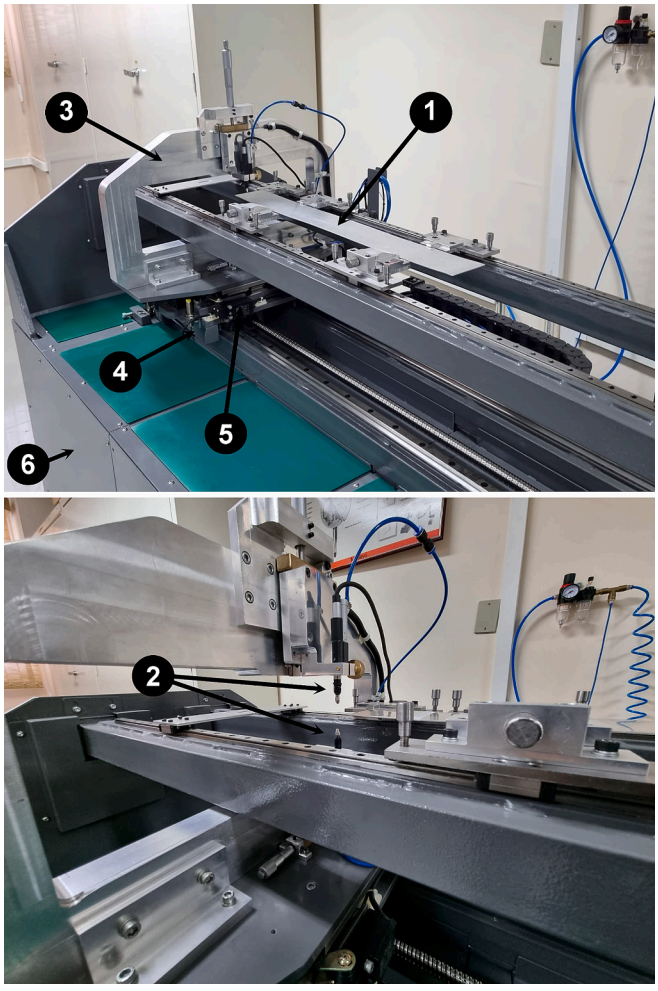

Fig. 6. Main components of the equipment: (1) Fuel plate, (2) Measurement sensor, (3) Measurement arch, (4) X-axis transporters, (5) Y-axis transporters, (6) Structural base.

2.2. Mathematical modeling

The development of data treatment for the measurements was guided by the creation of a mathematical model, grounded in statistical studies and the analysis of influencing factors in the system. As commented, the methodology expressed in the document JCGM 100:2008, titled "Evaluation of Measurement Data – Guide to the Expression of Uncertainty in Measurement," commonly known by the international acronym GUM [10,11], was used as a foundation.

This same mathematical treatment, which will be discussed below, was subsequently programmed, and validated using a spreadsheet software with a module for implementing commands in the programming language, in order to perform the same processing and analysis on all thickness points measured on the plates.

Initially, the modeling of the measurement phenomenon was developed with the aim of mathematically expressing the relationship between the output Y and the input variables X_i, for which Y has a functional relationship f, in the form:

$$Y = f(X_1, X_2, X_3, \cdots, X_n) \tag{04}$$

In the proposed method, the thickness of the fuel plate is determined by comparison with the thickness of a previously calibrated reference standard (gauge block) with the same nominal thickness. The direct output of the comparison between the measurement of the gauge block and the plate will be the difference in their thicknesses, that is:

$$Th_{pla} = Th_{std} + \Delta Th_{p-s} \tag{05}$$

where:

Th_{pla} = Thickness of the plate under measurement.

Th_{std} = Thickness of the reference standard (gauge block).

$\Delta Th_{p\text{-}s}$ = Difference between the thicknesses of the plate and the reference standard.

Based on equation (04), the modeling of the measurement phenomenon was developed to mathematically express the relationship between the output (measurement result) and the input quantities obtained from the developed measurement system.

The functional relationship between the measurand (plate thickness) and the other input quantities were based on knowledge of the equipment's structural data, information on the calibration standards used,

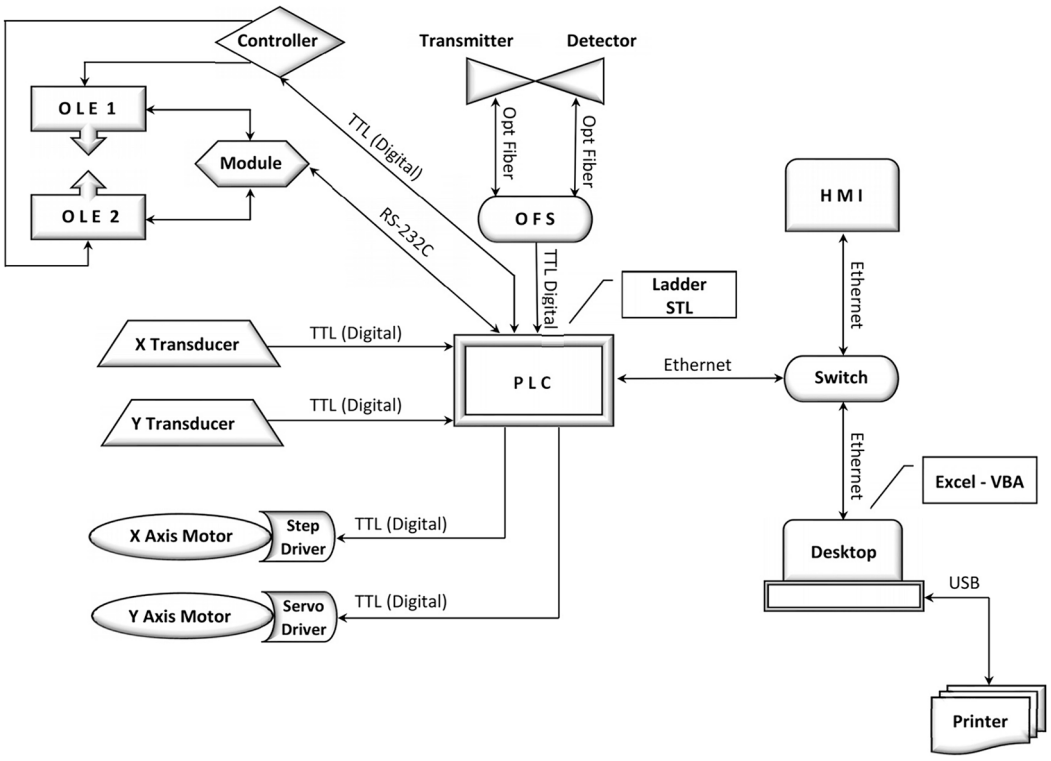

Fig. 7. System schematic diagram.

technical data obtained from the manufacturers of its components and environmental information available on the location of installation and operation of the equipment.

During the manufacture and assembly of the equipment, several adjustments were made, seeking to ensure maximum precision, minimizing geometric errors associated with its operation, thus guaranteeing the accuracy of the results. From these adjustments, information and values of the residual deviations were extracted, which served as the basis for developing the mathematical measurement model.

Thus, the following mathematical measurement model was established:

$$Th_{pla} = Th_{std} + \Delta Th_{p-s} + \delta S_{upp} + \delta S_{low} + \delta R_{ind} + \delta Te_{ref} + \delta Te_{p-s} + \delta F_{upp} + \\ + \delta F_{low} + \delta P_{gui} + \delta A_{pla} + \delta A_{p-s} \quad (06)$$

where:

Th_{pla} = Thickness of the plate under measurement.

Th_{std} = Thickness of the reference standard (gauge block).

$\Delta Th_{p\text{-}s}$ = Difference between the thicknesses of the plate and the reference standard.

δS_{upp} = Correction due to the maximum permissible error of the upper sensor.

δS_{low} = Correction due to the maximum permissible error of the lower sensor.

δR_{ind} = Correction due to the effect of the resolution of the integrated indication module.

δTe_{ref} = Correction due to the deviation from the reference temperature.

$\delta Te_{p\text{-}s}$ = Correction due to the temperature gradient effect between the plate and the standard.

δF_{upp} = Correction due to the effect of the measurement force from the upper sensor.

δF_{low} = Correction due to the effect of the measurement force from the lower sensor.

δP_{gui} = Correction due to the deviation of parallelism between the equipment guides.

δA_{pla} = Correction due to the deviation of alignment between the plate and the movement.

$\delta A_{p\text{-}s}$ = Correction due to the deviation of alignment between the plate and the reference standard.

2.3. Calculation of measurement results

The following example to illustrate the mathematical treatment developed is based on real data from thickness measurements of the fuel plate with serial number Si-1099, manufactured at the IPEN-CNEN/SP to compose a new fuel element to be used in the IEA-R1 Reactor,

Table 2
Data from fuel plate Si-1099 obtained in a real measurement situation.

repetitions (n)	values (mm) (y_i)
1	1.524
2	1.523
3	1.524
4	1.524
5	1.524
6	1.524
7	1.523
8	1.524
9	1.527
10	1.527
11	1.527
12	1.528
13	1.527
14	1.526
15	1.528
16	1.529
17	1.528
18	1.528
19	1.527
20	1.528

twenty thickness data points ($n = 20$) were considered at the coordinates X = 35.00 mm and Y = 112.50 mm, as shown in Table 2.

It is known that, referring to equation (04), what is practically obtained is an estimate of the measurand Y, now designated as y, using in this case the input estimates x_1, x_2, x_3, …, x_n, thus becoming:

$$y = f(x_1, x_2, x_3, \cdots, x_n) \tag{07}$$

From the data presented in Table 2, the measurement result, i.e., the estimate y of the measurand Y, was calculated based on the functional relationship f, using the obtained estimates x_i for the input quantities X_i.

It is assumed that the best available estimate of the expected value μy of a quantity y that varies randomly, and for which n independent observations y_i were made under the same repeatability conditions, is the arithmetic mean $\bar{y}$ of the n observations:

$$\bar{y} = \frac{1}{n}\sum_{i=1}^{n} y_i = 1.526mm \tag{08}$$

2.4. Assessment of standard uncertainties

For each of the input estimates x_i, a standard uncertainty $u(x_i)$ must be associated, which are obtained from a distribution of possible values of the input quantity X_i. This probability distribution can be based on frequency, i.e., on a series of observations X_{ik} of X_i, called Type A evaluation, or it can be a prior assumed frequency distribution, called Type B evaluation [10,11].

The Type A evaluation of standard uncertainty is inherent to the measurement process and is carried out through statistical treatment of a set of repeated measurements of the input quantity under repeatability conditions [23]. Thus, the experimental variance of the observations, which estimates the variance σ^2 of the probability distribution of x , is:

$$s^2(x_i) = \frac{1}{n-1}\sum_{i=1}^{n}(x_i - \bar{x})^2 \tag{09}$$

And the best estimate of the experimental variance of the mean $s^2(\bar{x})$, which quantifies how well $\bar{x}$ estimates the expectation μ_x of x , is:

$$s^2(\bar{x}) = \frac{s^2(x_i)}{n} \tag{10}$$

In situations where the uncertainty assessment of the input source is conducted using methods other than statistical, the methodology proposed by GUM refers to the evaluation of standard uncertainty as Type B.

Estimates of Type B standard uncertainty, $u(x_i)$, are made assuming that the values of x_i have a certain distribution and a range of dispersion. The distributions typically used according to the methodology are rectangular, triangular, "U" shaped, Gaussian, etc. [24]. In these cases, the assessment is developed through scientific judgment, relying on available information about the potential variability of x_i, which may include [10,11]:

- Measurement and prior test data;
- General knowledge of the behavior and properties of materials;
- Experience with the behavior and properties of instruments;
- Manufacturers specifications;
- Data provided in calibration certificates and other certificates;
- Uncertainties attributed to reference data extracted from handbooks.

2.5. Assessment of uncertainty contributions

The products between the standard uncertainty values u (x_i) and their respective sensitivity coefficients, c_i, give rise to the so-called uncertainty contribution, u_i (y), which corresponds to a measure of dispersion equivalent to a standard deviation, with the same unit of measurement as the measurand.

The partial derivatives $\partial f/\partial xi$ of each of the input quantities are called sensitivity coefficients c_i, and are used to mathematically describe how the output estimate Y varies with changes in the values of the input quantities x_i, as follows:

$$c_i \equiv \frac{\partial f}{\partial x_i}, \quad u_i(y) \equiv u(x_i)\,\mathrm{x}\,|c_i| \tag{11}$$

2.5.1. Uncertainty contribution associated with the difference between the thicknesses of the plate and the reference standard $(\Delta \mathbf{Th_{p-s}})$

The Type A evaluation of the standard uncertainty is the experimental standard deviation of the mean of the presented values, that is:

$$u_{x1} = u_A\left(\Delta Th_{p-s}\right) = \frac{s\,(x_i)}{\sqrt{n}} = \frac{2.00\,\mathrm{x}\,10^{-3}}{\sqrt{20}} = 4.47\,\mathrm{x}\,10^{-4}\,mm \tag{12}$$

2.5.2. Uncertainty contribution associated with the thickness of the reference standard (gauge block) (Th_{std})

In the calibration certificate of the standard reference block used to adjust the equipment, it is stated that the nominal deviation found is + 0.10 μm, with the uncertainty of this calibration being ± 0.06 μm. Considering the magnitude of the values to be of little significance, in this development, we chose not to make corrections to this deviation value. Therefore, the value of ± 0.16 μm is used for the composition of this uncertainty contribution.

The certificate number 12,689 was issued by the CAL 0031 laboratory, accredited by the National Institute of Metrology, Quality, and Technology (INMETRO), and therefore, part of the Brazilian Calibration Network (RBC). Through this calibration certificate and the proposed methodology, it is demonstrated that the measurement results obtained from the equipment are traceable, making it possible to relate them to a national reference standard through an uninterrupted and documented chain of calibrations.

In the same certificate, it is stated that the reported expanded measurement uncertainty is declared as the standard uncertainty of the measurement multiplied by the coverage factor $k = 2.00$, which, for a normal distribution, corresponds to an approximate coverage probability of 95 %. Thus, the standard uncertainty will be:

$$u_{x2} = u_B\left(Th_{std}\right) = \frac{U\left(Th_{std}\right)}{k} = \frac{1.60\,\mathrm{x}\,10^{-4}}{2} = 8\,\mathrm{x}\,10^{-5}\,mm \tag{13}$$

2.5.3. Uncertainty contribution associated with the maximum permissible error of the sensors (S_{sen})

In the calibration of the OLE sensors, carried out in our laboratory, using certified standard blocks, an expanded uncertainty of ± 2 μm was found, which is the standard uncertainty of the measurement multiplied by the coverage factor k = 2.00, which, for a normal distribution corresponds to a coverage probability of approximately 95 %. Thus, the standard uncertainty will be:

$$u_{x3.4} = u_B\left(S_{sen}\right) = \frac{(S_{sen})}{k} = \frac{\left(2.00\,\mathrm{x}\,10^{-3}\right)}{2} = 1.00\,\mathrm{x}\,10^{-3}\,mm \tag{14}$$

2.5.4. Uncertainty contribution associated with the effect of resolution provided by the integrated indication and communication module of the sensors (R_{ind})

The specifications handbook for the integrated indication and communication module states that the quantization error (deviation) declared by the manufacturer is ± 1 significant digit, which in our case is equivalent to 1 μm [25]. As there is no available information on the input quantity R_{ind} regarding possible values of x_i within the interval, a rectangular and symmetrical probability distribution is assumed. Thus, the standard uncertainty will be:

$$u_{x5} = u_B\left(R_{ind}\right) = \frac{(R_{ind})}{\sqrt{3}} = \frac{1.00\,\mathrm{x}\,10^{-3}}{\sqrt{3}} = 5.77\,\mathrm{x}\,10^{-4}\,mm \tag{15}$$

2.5.5. Uncertainty contribution associated with the effect of deviation from laboratory reference temperature (Te_{ref})

During the tests, a maximum deviation of ± 1.5 °C was detected during the measurement period. As there is no available information on the input quantity δTe_{ref} regarding possible values of x_i within the interval, a rectangular and symmetrical probability distribution is assumed. Thus, the standard uncertainty will be:

$$u_{x6} = u_B\left(Te_{ref}\right) = \frac{\left(Te_{ref}\right)}{\sqrt{3}} = \frac{1.5}{\sqrt{3}} = 8.66 \times 10^{-1}\,^{\circ}\mathrm{C} \quad (16)$$

The effect of the deviation from the laboratory temperature during measurement, in relation to the laboratory reference temperature of 20 °C [26], is determined by the product of three factors: (a) the distance between the sensor's height adjustment supports and the plate, in our case equal to 40.6 mm L_{sen}, (b) the temperature deviation occurred during the measurement period ΔTe_{ref}, and (c) the difference between the linear expansion coefficients of the sensor materials (stainless steel) and the measuring arc (aluminum) of the equipment $\Delta\alpha_{mat}$, namely:

$$\Delta L = 2\,\mathrm{x}\,L_{sen}\,\mathrm{x}\,\Delta Te_{ref}\,\mathrm{x}\,\Delta\alpha_{mat} \quad (17)$$

Thus, its sensitivity coefficient c_6 will be 3.65 × 10^{-4} mm/°C.

2.5.6. Uncertainty contribution associated with the temperature gradient effect on the plate and the standard (Te_{p-s})

During the tests, a maximum gradient of 3 °C was detected between the plate and the reference standard during the measurement period. As there is no available information on the input quantity $\delta Te_{p\text{-}s}$ regarding possible values of x_i within the interval, a rectangular and symmetrical probability distribution is assumed. Thus, the standard uncertainty will be:

$$u_{x7} = u_B\left(Te_{p-s}\right) = \frac{\left(Te_{p-s}\right)}{\sqrt{3}} = \frac{3}{\sqrt{3}} = 1.73\,\mathrm{x}\,10^{+0}\,^{\circ}\mathrm{C} \quad (18)$$

The effect of the gradient from the plate temperature, in relation to the reference standard (gauge block) temperature during measurement, is determined by the product of three factors: (a) the thickness of the reference standard, in our case equal to 1.5 mm Th_{std}; (b) the temperature gradient between the plate and the standard occurred during the measurement period $\Delta Te_{p\text{-}s}$; and (c) the linear expansion coefficients of the material of the plate α_{pla}, namely:

$$\Delta L = Th_{std}\,x\,\Delta Te_{p-s}\,x\,\alpha_{pla} \quad (19)$$

Thus, its sensitivity coefficient c_7 will be 3.53 × 10^{-5} mm/°C.

2.5.7. Uncertainty contribution associated with the effect of the measurement force of the sensors (F_{sen})

In the technical specifications provided by the manufacturer of the sensors, it is stated that the maximum measuring force exerted during measurement in the vertical position is 0.8 N, or 81.58 gf, and this value may vary depending on the sensor installation position. As it is a measuring force, with the highest probability of occurrence near the specified limit values, a "U" shaped probability distribution was assumed [27] for this input quantity δF_{sen}, like so:

$$u_{x8.9} = u_B\left(F_{sen}\right) = \frac{\left(F_{sen}\right)}{\sqrt{2}} = \frac{8.16\,\mathrm{x}\,10^{+1}}{\sqrt{2}} = 5.77\,\mathrm{x}\,10^{+1}\mathrm{gf} \quad (20)$$

The effect of the variation in the measuring force on the sensors, can be calculated according to the formula developed by Puttock and Thwaite [28], where, for the determination of the deformation due to the compression force of the sensor's contact sphere on the plate surface, the following factors are considered:

$$\Delta L = \frac{(3\pi)^{\frac{2}{3}}}{2}\,\mathrm{x}\,F_{sen}{}^{\frac{2}{3}}\,\mathrm{x}\,(V_1 + V_2)^{\frac{2}{3}}\,\mathrm{x}\left(\frac{1}{d}\right)^{\frac{1}{3}} \quad (21)$$

where:

ΔL = Deformation occurred.

F_{sen} = Sensor measurement force = 0.8 N = 81.58 gf.

d = Diameter of the sensor contact sphere = 3 mm.

$V = \frac{(1-\sigma_n^2)}{\pi}\mathrm{x}\epsilon_n$

σ_1 = Poisson's ratio of aluminum = 0.33

σ_2 = Poisson's ratio of tungsten carbide = 0.28

ϵ_1 = Elastic modulus of aluminum = 69.0 GPa = 7,036,042 gf/mm^2

ϵ_2 = Elastic modulus of tungsten carbide = 619.5 GPa = 63,171,419 gf/mm^2

Substituting the values, we can simplify equation (21) to:

$\Delta L = F_{sen}{}^{\frac{2}{3}}\mathrm{x}1.95573x10^{-5}$ (22)

Thus, its sensitivity coefficient $c_{8.9}$ will be 4.51 × 10^{-6} mm/gf.

2.5.8. Uncertainty contribution associated with deviation in parallelism between equipment guides (P_{gui})

Based on the measurements performed on the equipment during its assembly phase, it was found that parallelism deviations between the two displacement guides on the Y and X axes could result in rolling movements during the translation movement of these axes, producing cosine errors in the measurements.

After adjusting to achieve the best possible alignment between the displacement guides, a residual parallelism deviation of 0.05 mm was observed on the Y-axis between the two linear guides over the 960 mm travel of the axis. Considering that the distance between the guides on this axis is 170 mm, this residual deviation θ_{gui} can be expressed as approximately 2.94 × 10^{-4} rad.

No significant parallelism deviations (greater than 0.001 mm) were detected in measurements on the X-axis between the two linear guides over the 110 mm travel of the axis.

Since this is an angular deviation, which is frequently identified in dimensional metrology as a source of cosine error, and is characterized by occurrence on only one side of the interval, a "U" shaped probability distribution was assumed [27] for this input quantity δP_{gui}, as follows:

$$u_{x10} = u_B\left(P_{gui}\right) = \frac{\left(P_{gui}\right)}{\sqrt{2}} = \frac{\frac{2.94\,\mathrm{x}\,10^{-4}}{2}}{\sqrt{2}} = 1.04\,\mathrm{x}\,10^{-4}\,rad \quad (23)$$

The effect of the deviation in parallelism between the equipment guides is given by the difference between the value of the plate thickness Th_{pla} and the value of the plate thickness measured with an inclination θ_{gui}, that is:

$\Delta L = Th_{pla}\mathrm{x}(1 - \cos\theta_{gui})$ (24)

Thus, its sensitivity coefficient c_{10} will be 4.41 × 10^{-4} mm/rad.

2.5.9. Uncertainty contribution associated with misalignment between the plate and the axis movement of the equipment (A_{pla})

During the assembly of the equipment, it was also found that alignment deviations between the movement of the measurement sensors and the surface of the plate being measured could also cause cosine errors in the measurements. Adjustments were made to achieve the best possible alignment between the support faces of the plate positioners and the movements executed by the X and Y axis transporters.

After the necessary adjustments, it was observed that the maximum residual value obtained in the alignment deviation between the surface of the plate being measured and the movement of the measurement sensors was 0.15 mm over a distance of 140 mm, which corresponds to an angular deviation θ_{pla} of approximately 1.07 × 10^{-3} rad.

It was also observed that the obtained values were also influenced by flatness deviations of the plate and possible flexions caused by the force of gravity. To minimize the deflection caused by its own weight during measurement, the plates are positioned at their respective Bessel points [29], through the correct positioning of the adjustable support elements.

Since it is an angular deviation, often identified in dimensional metrology as a source of cosine error, characterized by occurrence on

only one side of the interval, a "U" shaped probability distribution was assumed [27] for this input quantity δA_{pla}, as follows:

$$u_{x11} = u_B\left(A_{pla}\right) = \frac{\left(A_{pla}\right)}{\sqrt{2}} = \frac{\frac{1.07\,x\,10^{-3}}{2}}{\sqrt{2}} = 3.79\,x\,10^{-4} rad \quad (25)$$

The effect of the misalignment between the plate and the movement of the equipment axes is given by the difference between the value of the plate thickness Th_{pla} and the value of the plate thickness measured with the inclination θ_{pla}, caused by the misalignment between the plate and the movement of the equipment axes, that is:

$$\Delta L = Th_{pla}\,x\,\left(1 - \cos\theta_{pla}\right) \quad (26)$$

Thus, its sensitivity coefficient c_{11} will be 1.61 × 10^{-3} mm/rad.

2.5.10. Uncertainty contribution associated with misalignment between the plate and the standard (A_{p-s})

In addition, during the equipment assembly stage, it was noted that misalignments between the normal axis of the plane of the reference standard and the normal axis of the plane formed by the support faces of the plate positioners could induce cosine errors in measurements referenced during the calibration process.

After adjusting to achieve the best possible alignment between the planes, it was observed that the maximum residual misalignment deviation between the axis of the plane formed by the support faces of the plate positioners and the axis of the plane of the standard surface was 0.05 mm over the 25 mm useful length of the largest standard used. This corresponds to an angular deviation $\theta_{p\text{-}s}$ of approximately 2.00 × 10^{-3} rad.

Since it is an angular deviation, often identified in dimensional metrology as a source of cosine error, characterized by occurrence on only one side of the interval, a "U" shaped probability distribution was assumed [27] for this input quantity $\delta A_{p\text{-}s}$, as follows:

$$u_{x12} = u_B\left(A_{p-s}\right) = \frac{\left(A_{p-s}\right)}{\sqrt{2}} = \frac{\frac{2.00\,x\,10^{-3}}{2}}{\sqrt{2}} = 7.07\,\times\,10^{-4}\,rad \quad (27)$$

The effect of the misalignment between the axes of the plate and the standard is given by the difference between the value of the plate thickness Th_{pla} and the value of the plate thickness measured with the inclination $\theta_{p\text{-}s}$, caused by the misalignment between the axes of the planes of the plate and the standard, that is:

$$\Delta L = Th_{pla}\,x\,\left(1 - \cos\theta_{p-s}\right) \quad (28)$$

Thus, its sensitivity coefficient c_{12} will be 3.00 × 10^{-3} mm/rad.

For better visualization, the information on the input quantities and their respective values that compose the evaluation of the uncertainty contributions are summarized in Table 3 according to the calculations previously developed.

From the obtained results, it can be observed that the input quantities associated with the deviations of parallelism between the equipment guides P_{gui}, alignment between the plate and the movement A_{pla}, and alignment between the plate and the standard $A_{p\text{-}s}$ did not present uncertainty contributions of significant magnitude compared to others.

Thus, for reducing computational analysis volume, it was decided to disregard them in the development of the algorithm for data treatment and modeling, as well as in the definition of the final mathematical model for uncertainty analysis calculation of measurement results.

Therefore, the mathematical model of the measurement described in equation (06) becomes:

$$Th_{pla} = Th_{std} + \Delta Th_{p-s} + \delta S_{upp} + \delta S_{low} + \delta R_{ind} + \delta Te_{ref} + \delta Te_{p-s} + \\ + \delta F_{upp} + \delta F_{low} \quad (29)$$

2.6. Assessment of associated covariances

Possible covariances and the respective Pearson correlation coefficients r of the input quantities of the proposed model (equation 29) were evaluated according to equation (30) and presented in Table 4.

$$r\left(x_i, x_i^{'}\right) = \frac{s\left(x_i, x_i^{'}\right)}{\sqrt{s\left(x_i, x_i\right)\,x\,s\left(x_i^{'}, x_i^{'}\right)}} \quad (30)$$

A significance test was carried out with the values in Table 4, according to the following hypotheses:

$H_0 : \rho = 0$

$H_1 : \rho \neq 0$

$$t_0 = \frac{r\,x\,\sqrt{n-2}}{\sqrt{1-r^2}} \quad (31)$$

The highest correlation coefficient evaluated was 0.12, found between the input quantities δTe_{ref} and δR_{ind}, as follows:

$$t_0 = \frac{0.12\,x\,\sqrt{20-2}}{\sqrt{1-0.12^2}} = 0.513 \quad (32)$$

The critical value of t_c for 5 % significance level α and 18 degrees of freedom $\nu = n\text{-}2$ is:

Table 4
Pearson correlation coefficients r between input quantities.

Input Quant (xi)	δF_{low}	δF_{upp}	δTe_{p-s}	δTe_{ref}	δR_{ind}	δS_{low}	δS_{upp}
Th_{std}	0.01	−0.01	0.02	−0.04	0.04	−0.01	−0.03
δS_{upp}	−0.07	0.11	0.06	−0.07	−0.04	0.03	– – –
δS_{low}	−0.09	0.11	0.02	0.07	0.04	– – –	– – –
δR_{ind}	−0.08	0.03	0.04	0.12	– – –	– – –	– – –
δTe_{ref}	0.02	−0.02	0.06	– – –	– – –	– – –	– – –
δTe_{p-s}	−0.05	−0.09	– – –	– – –	– – –	– – –	– – –
δF_{upp}	0.10	– – –	– – –	– – –	– – –	– – –	– – –

Table 3
Assessment of uncertainty contributions.

Input QuantityX_i	Estimate of Quantityx_i	Standardized Uncertainty$u(x_i)$	Probability Distribution	Sensitivity Coefficient$\lvert c_i \rvert$	Uncertainty Contribution (mm)$u_i(y)$
ΔTh_{p-s}	0.026	4.47 × 10^{-04}	normal	1	0.00045
Th_{std}	1.500	8.00 × 10^{-05}	normal	1	0.00008
δS_{upp}	0	1.00 × 10^{-03}	normal	1	0.00100
δS_{low}	0	1.00 × 10^{-03}	normal	1	0.00100
δR_{ind}	0	5.77 × 10^{-04}	rectangular	1	0.00058
δTe_{ref}	0	8.66 × 10^{-01}	rectangular	3.65 × 10^{-04}	0.00032
δTe_{p-s}	0	1.73 × 10^{+00}	rectangular	3.53 × 10^{-05}	0.00006
δF_{upp}	0	5.77 × 10^{+01}	"U" shaped	4.51 × 10^{-06}	0.00026
δF_{low}	0	5.77 × 10^{+01}	"U" shaped	4.51 × 10^{-06}	0.00026
δP_{gui}	0	1.04 × 10^{-04}	"U" shaped	4.41 × 10^{-04}	0.00000
δA_{pla}	0	3.79 × 10^{-04}	"U" shaped	1.61 × 10^{-03}	0.00000
δA_{p-s}	0	7.07 × 10^{-04}	"U" shaped	3.00 × 10^{-03}	0.00000

$$t_c = t_{\alpha/2,\nu} = 2.101 \quad (33)$$

Since $t_0 < t_c$, the null hypothesis is accepted, and it is concluded that there is sufficient evidence to affirm that there are no significant correlations between the input quantities.

In other words, the inputs can be considered independent from each other, and therefore, the expression for the combined variance $u_c^2(y)$ associated with the measurement result will be:

$$u_c^2(y) = \sum_{i=1}^{N} \left[\frac{\partial f}{\partial x_i}\right] u^2(x_i) \quad (34)$$

2.7. Determination of the combined standard uncertainty

Thus, the combined standard uncertainty $u_c(y)$ will be the positive square root of the combined variance $u_c^2(y)$, that is:

$$u_c(y) = u_c(Th_{pla}) =$$

$$= \sqrt[2]{\left(\begin{array}{c} 0.00045^2 + 0.00008^2 + 0.00100^2 + 0.00100^2 + 0.00058^2 + 0.00032^2 + \\ +0.00006^2 + 0.00026^2 + 0.00026^2 \end{array}\right)}$$

$$u_c(Th_{pla}) = 0.00167mm \quad (35)$$

2.8. Calculation of expanded uncertainty

Next, the calculation of the effective degrees of freedom was performed based on the individual degrees of freedom of the individual uncertainty contributions, using the Welch-Satterthwaite equation, as follows:

$$\upsilon_{eff} = \frac{u_c^4(y)}{\sum_{i-1}^{N} \frac{u_i^4(y)}{\upsilon_i}} = \frac{0.00167^4}{\frac{0.00045^4}{19}} = 3,668 \quad (36)$$

After obtaining the effective degrees of freedom ν_{eff} of the combined standard uncertainty $\boldsymbol{u_c\ (Th_{pla})}$, the coverage factor $\boldsymbol{k}$ was determined from the Student's $\boldsymbol{t}$-distribution, assuming a coverage probability of 95 %, as follows:

$$k_{95} = t_{95}(3,668) = 2.0 \quad (37)$$

The methodology proposed by the GUM [10,11] emphasizes that, due to the extent and reliability of the available information, it is rarely justifiable to process a large volume of data required to combine probability distributions. Instead, it is acceptable to use an approximation for the distribution of the output quantity.

Thus, considering the Central Limit Theorem (CLT), it is sufficient to assume that the probability distribution of $(y\text{-}Y)/u_c(y)$ is the t-distribution and take $k_p = t_p\ (\nu_{eff})$, with the t-factor based on the effective number of degrees of freedom ν obtained by the Welch-Satterthwaite equation. Therefore, the expanded uncertainty is obtained:

$$U_{95}(Th_{pla}) = u_c(Th_{pla}) \text{ x } k_{95}$$

$$U_{95}(Th_{pla}) = 0.00167 \text{ x } 2.0 \cong 0.003\,mm \quad (38)$$

2.9. Report of measurement results

Finally, it is possible to declare the measurement result of the measured point as:

$$Th_{pla} = (1.526 \pm 0.003)\,mm \quad (39)$$

The reported measurement uncertainty is declared as the expanded uncertainty, which is the standard uncertainty of the measurement multiplied by the coverage factor $\boldsymbol{k = 2.0}$, which, for a $\boldsymbol{t}$-distribution with $\boldsymbol{\nu_{eff} = 3,668}$ effective degrees of freedom, corresponds to a coverage probability of approximately 95 %.

3. Measurements

After the functional tests were completed and the data processing methods were defined, a series of measurements were started under laboratory conditions, with the aim of studying the metrological response of the new measurement system developed.

The first measurements performed were aimed at observing the performance of the equipment and analyzing the results obtained by evaluating the stability, drift, and instrumental bias of the system, and systematically analyzing the uncertainty obtained in the results, by applying the presented mathematical model.

For the validation of the new measurement system, IPEN-CNEN/SP provided two plates with manufacturing codes Si-1097 and Si-1099, manufactured to be part of the fuel elements used in the IEA-R1 nuclear research reactor. Additionally, two plates with manufacturing codes IPMB-007 and IPMB-010, manufactured for use in the IPEN/MB-01 nuclear research reactor, were made available.

The equipment allows the user to define, via programming, the number of points to be measured on each fuel plate. These points are located according to a coordinate system defined along the plate plane.

The sum of the measured points is denominated (N_p) and results from a measurement matrix adopted in the X-Y plane of the system. This matrix consists of a number of columns (N_X) identified by their coordinates on the X-axis (width of the plate) and a number of rows (N_Y) identified by their coordinates on the Y-axis (length of the plate).

When all the measurement points determined by the matrix are measured, a measurement cycle is completed and, to carry out a statistical analysis of the collected data, repetitions of these measurement cycles are executed. The number of these repetitions cycles (N_c) determines the sample size obtained at each of the measured points.

Completing all predefined measurement cycles allows the calculation development to present the plate thickness results and characterizes a complete series of measurements with (N_d) collected data.

$$N_X \text{ x } N_Y = N_p \quad (40)$$

$$N_p \text{x} N_c = N_d \quad (41)$$

where:

N_X = Number of columns
N_Y = Number of rows
N_p = Number of measured points
N_c = Number of measurement cycles
N_d = Number of collected data

Three measurement campaigns were carried out. The first measurement campaign aimed to observe the behavior and performance of the equipment, as well as to evaluate the results obtained on each of the four different plates analyzed. To provide future parameters for analysis and comparisons, it was chosen, in this campaign, to collect the data in the same positions determined by the procedures that guide manual measurements performed with micrometers.

Thus, in the first measurement campaign, four complete

measurement series (1 per plate) were carried out. In each series, 5 measurement cycles ($N_c = 5$) were performed, and 21 thickness points ($N_p = 21$) were measured in each cycle, totaling 420 data collected for treatment and analysis in this campaign.

In the second measurement campaign, the aim was to observe the equipment's behavior in response to changes in sample size within each measurement series and the effects these sample variations could have on its results. For this campaign, the plate with manufacturing code Si-1099 was randomly selected as the measurement object. Nineteen complete measurement series were conducted, where measurement cycles ranged from 02 to 20 ($N_c = 02 \sim 20$), measuring 21 thickness points on the plate in each cycle ($N_p = 21$). This resulted in 4,389 collected data points for processing and analysis in this second campaign.

In the third measurement campaign, the aim was to observe the equipment's behavior with a change in the number of thickness measurement points on the plates and determine if this alteration could have a significant effect on the results. For this measurement campaign, the plate with manufacturing code Si-1097 was randomly selected. With this purpose, three complete measurement series were conducted. In each of the series 5 measurement cycles ($N_c = 5$) were performed, and the measured thickness points varied between 21, 39, and 75 points ($N_p = 21; 39; 75$) in each series. This resulted in 675 collected data points for treatment and analysis in this final measurement campaign.

Thus, in this study, 26 complete measurement series were conducted, comprising the execution of 244 measurement cycles, and resulting in 5,484 collected data points for treatment and analysis. At the end of each measurement, the equipment automatically generates a measurement report that includes the report number, location and date of the measurement, the object and objectives of the measurement, the method description, and the standards used.

The report results include the minimum, average, and maximum thickness values, as well as the variations encountered. A deviation graph relating thickness values to obtained uncertainties and the respective specification intervals for each fuel plate is also presented. Information regarding the measurement execution, including temperatures, execution time, and the technician responsible for the measurement, is recorded.

The same programming algorithm developed was also prepared to generate chromatic response curves of the thickness variation of the plates.

4. Results and discussion

4.1. Obtained values and uncertainties

Table 5 presents the results of the fuel plate thickness measurements performed on the new equipment and their respective uncertainties calculated by the system.

By examining the results, it is observed that the obtained uncertainty values remained constant at ± 3 μm across all 25 series conducted with 3 or more measurement cycles ($N_c = 3 \sim 20$). Only in the series performed with 2 measurement cycles ($N_c = 2$), a slight increase in the uncertainty value was observed, reaching ± 4 μm. This result was expected, considering the low statistical representativity obtained with only 2 samples per measured point.

Fig. 8 shows that the number of measurement cycles has a greater influence on the values of the expanded uncertainties U_{95} and the coverage factors k between samples of size 2 up to 4 ($N_c = 2 \sim 4$). From 5 samples, the indicators suffer minor variation with the increase in sampling.

It was verified that there was no variation in the equipment's behavior in response to the alteration of the number of thickness points measured on the fuel plates. There were no significant variations among the results of the series conducted with 21, 39, or 75 points ($N_p = 21; 39; 75$) per cycle. The values of minimum and maximum thickness, as well as the measurement uncertainty, remained constant.

Only the average thickness value varied between 1.484 mm ($N_p = 21$) and 1.487 mm ($N_p = 75$). This variation can be explained by considering that the absence of the fuel core at the plate's end results in slightly smaller thicknesses at the edges. The increase in the number of measurement points causes the number of points measured at the plate's

Table 5
Measurements results and calculated uncertainties.

Fuel Plate ID	Number of Points Measured (N_p) (per cycle)	Number of Measuring Cycles (N_c) (sampling)	Number of Collected Data (N_d)	Plate Thickness(mm)			Measurement Uncertainty (U_{95}) (mm)
				Minimum	Mean	Maximum	
Si-1097	21	5	105	1.470	1.484	1.498	± 0.003
Si-1099	21	5	105	1.498	1.533	1.551	± 0.003
IPMB-007	21	5	105	1.355	1.362	1.366	± 0.003
IPMB-010	21	5	105	1.349	1.358	1.368	± 0.003
Si-1099	21	2	42	1.498	1.533	1.551	± 0.004
Si-1099	21	3	63	1.498	1.533	1.551	± 0.003
Si-1099	21	4	84	1.498	1.533	1.551	± 0.003
Si-1099	21	5	105	1.498	1.533	1.551	± 0.003
Si-1099	21	6	126	1.498	1.533	1.551	± 0.003
Si-1099	21	7	147	1.498	1.533	1.551	± 0.003
Si-1099	21	8	168	1.498	1.533	1.551	± 0.003
Si-1099	21	9	189	1.498	1.533	1.551	± 0.003
Si-1099	21	10	210	1.498	1.533	1.551	± 0.003
Si-1099	21	11	231	1.498	1.533	1.551	± 0.003
Si-1099	21	12	252	1.498	1.533	1.551	± 0.003
Si-1099	21	13	273	1.498	1.533	1.551	± 0.003
Si-1099	21	14	294	1.498	1.533	1.551	± 0.003
Si-1099	21	15	315	1.498	1.533	1.551	± 0.003
Si-1099	21	16	336	1.498	1.533	1.552	± 0.003
Si-1099	21	17	357	1.498	1.533	1.552	± 0.003
Si-1099	21	18	378	1.498	1.533	1.552	± 0.003
Si-1099	21	19	399	1.498	1.533	1.552	± 0.003
Si-1099	21	20	420	1.498	1.533	1.552	± 0.003
Si-1097	21	5	105	1.470	1.484	1.498	± 0.003
Si-1097	39	5	195	1.470	1.486	1.498	± 0.003
Si-1097	75	5	375	1.470	1.487	1.498	± 0.003
Total		244	5,484				

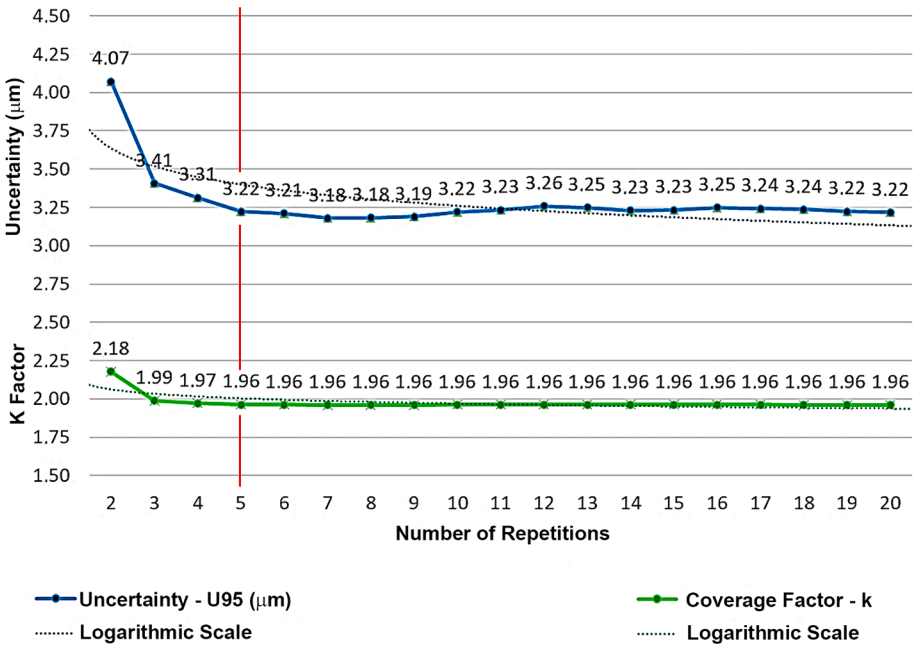

Fig. 8. Analysis of the effect of the number of measurement cycles on the results.

edges to decrease proportionally in relation to the number of more central points considered, slightly raising the average value.

The analysis of the obtained data, correlating the values of combined standard uncertainties u_c, effective degrees of freedom ν_{eff}, and coverage factors k with the number of repetitions (Fig. 8), confirms the consistency of the proposed mathematical modeling and verifies the correct correlations with the influencing factors. It reveals a sufficient understanding of the phenomena involved in the measurement performed by the equipment.

Regarding process efficiency and analysis speed, it was observed that the average time for the execution of a complete measurement cycle, using a 3 × 7 matrix (21 points per cycle), decreased from 20 min in the manual method with micrometers to 3 min and 20 s with the new automated system.

4.2. Equipment precision (Repeatability)

In addition to measurements performed on the four fuel plates, the precision of the equipment was also studied by assessing its repeatability. At the beginning of each measurement series, sensor adjustment (or preset) was performed using a reference standard class "0"gauge block [30], whose thickness was equal to the nominal thickness value of the fuel plate to be measured. After the completion of the first cycle of measurements, and in all subsequent measurement cycles of the same series, the equipment received a command to return to the sensor adjustment point, where the device's response value for the thickness indication of the standard block was verified. This verification was performed 218 times. The amplitude relative to the preset value performed at the beginning of each series was $\hat{r} = 2\mu m$, and the sample standard deviation was $s_x = 0.7577\mu m$. In view of these results, it was decided to assume that the representative value of the precision (repeatability) of the equipment is 2 μm (2σ).

It can be observed that the value found is quite consistent in order of magnitude, when correlated with the values of the data extracted from the uncertainty calculations of the plate measurements presented in Table 6.

The repeatability value of 2 μm (2σ) also shows good agreement when correlated with the maximum value of the quantization error (deviation) of the sensor system specified by the manufacturer, which is ± 1 significant digit, which in our case is equivalent to 1 μm [25].

To control the displacement of the X and Y axes, incremental linear transducers were employed, whose characteristics are presented in Table 7 [31].

Table 6
Measurement uncertainty calculations.

ID Fuel Plate	Combined Standard Uncertainty U_c (μm)	Effective Degrees of Freedom ν_{eff}	Coverage Factor k	Expanded Uncertainty U_{95} (μm)
Si 1097	1.71	178	1.97	± 3.38
Si 1099	1.64	725	1.96	± 3.22
IPMB 007	1.68	278	1.97	± 3.31
IPMB 010	1.76	106	1.98	± 3.49

Table 7
Specifications of X and Y linear displacement scales (transducers).

Displacement axis	Transducer model	Measuring Interval (mm)	Resolution (μm)	Maximum permissible error M_{PE} (μm)
X	M2X 170	170	1	± 5
Y	M2X 1140	1,140	1	± 5

Table 8
Calculations of measurement capability indices for the equipment

ID Fuel Plate	Specification interval (thickness tolerance) S_I (μm)	2 x Expanded Uncertainty 2 x U_{95} (μm)	Measurement Capability Index C_m
Si-1097	(1.620–1.470) = 150	(2 × 3.38) = 6.76	22.19
Si-1099	(1.620–1.470) = 150	(2 × 3.22) = 6.44	23.29
IPMB-007	(1.370–1.330) = 40	(2 × 3.31) = 6.62	6.04
IPMB-010	(1.370–1.330) = 40	(2 × 3.49) = 6.98	5.73

4.3. Measurement capability of the equipment

Applying the theory presented in the introduction section, the measurement capability indices of the equipment C_m were calculated according to the data from each fuel plate measured, as shown in Table 8.

The conducted measurement capability analyses indicate that, in all measurements performed, values of indices equal to or greater than five were achieved ($C_m \geq 5$). This implies that the expanded uncertainties obtained in the measurement results were always equal to or less than 10 % of the specification interval S_I (thickness tolerance requirements) of the analyzed fuel plates, a proportion considered suitable for our application.

5. Conclusions

In a comprehensive study comprising 25 measurement series, each conducted with three or more measurement cycles ($Nc \geq 3$), the expanded uncertainty of the measurement U_{95} consistently remained within $\pm$ 3 μm. This observation underscores that the accuracy, resolution, and sensitivity of the newly developed measurement equipment align with the design and project requirements. The presented results demonstrate that the system exhibits adequate precision for its intended application, maintaining a dispersion value of measurements at 2 μm (2σ) under repeatability conditions. This value also indicates good stability and minimal instrumental drift.

In summary, the metrological study confirms that the novel automated fuel plate measurement system successfully achieves its proposed objective. Compared to previously employed method, it enhances metrological reliability, flexibility, and productivity gains in the conformity assessment processes during the manufacturing of fuel plates at IPEN-CNEN/SP.

CRediT authorship contribution statement

Marcelo Kobayoshi: Validation, Resources, Methodology, Investigation, Formal analysis, Data curation. **Ricardo Mendes Leal Neto:** Writing – review & editing, Methodology, Formal analysis. **Elita Fontenele Urano de Carvalho:** Writing – review & editing, Visualization. **Michelangelo Durazzo:** Writing – original draft, Validation, Supervision, Project administration, Formal analysis, Conceptualization.

Declaration of competing interest

The authors declare that they have no known competing financial interests or personal relationships that could have appeared to influence the work reported in this paper.

Data availability

Data will be made available on request.

Acknowledgments

The authors are grateful to São Paulo Research Foundation (FAPESP) for the research grant 2021/14331-5. The authors would also like to thank CNPq (National Council for Scientific and Technological Development) for the research grant 309826/2021-7 provided for this work.

References

[1] M. Durazzo, P.E. Umbehaun, W.M. Torres, J.A.B. Souza, D.G. Silva, D.A. Andrade, Procedures for manufacturing an instrumented nuclear fuel element, Prog Nucl Energy 113 (2019) 166–174, https://doi.org/10.1016/j.pnucene.2019.01.021.

[2] J.A. Perrotta, I.J. Obadia, The RMB Project development status. in: Proceedings of International Conference on Research Reactors: Safe management and effective utilization. session C: New research reactor projects. 14-18 November 2011, Rabat, Morocco. Proceedings series. International Atomic Energy Agency. 2012. STI/PUB/1575 978-92-0-184610-5 (available at https://www-pub.iaea.org/MTCD/Publications/PDF/P1575_CD_web/datasets/abstracts/C6Perrotta.html.

[3] J.A. Perrotta, A.J. Soares, RMB: The new Brazilian multipurpose research reactor. in: Proceeding of International Topical Meeting on Research Reactor Fuel Management RRFM 2014, Ljubljana, Slovenia, 20 March – 3 April, P. 394-401, 2014 (available at https://www.euronuclear.org/download/proceedings-rrfm-2014/.

[4] M. Durazzo, H.G. Riella, Procedures for manufacturing nuclear research reactor fuel elements, Lambert Academic Publishing, Saarbrucken, 2015, p. 242.

[5] A.R. Kaufman, Nuclear reactor fuel elements, metallurgy, and fabrication, Interscience, New York, N.Y., 1962.

[6] C.E. Weber, H.H. Hirsch, Dispersion-type fuel elements: in Proceedings of the International Conference on the Peaceful Uses of Atomic Energy, Geneve, Switzerland, August 8-20, 1955.Paper No. P/561.

[7] M. Durazzo, E. Vieira, E.F.U. Carvalho, H.G. Riella, Evolution of fuel plate parameters during deformation in rolling, J. Nucl. Mater. 490 (2017) 197–210, https://doi.org/10.1016/j.jnucmat.2017.04.018.

[8] International Atomic Energy Agency-IAEA, Standardization of specifications and inspection procedures for LEU plate-type research reactor fuels, Vienna, 1988, 35 p. IAEA-TECDOC-467 (available at https://www-pub.iaea.org/MTCD/Publications/PDF/te_467_prn.pdf.

[9] International Atomic Energy Agency-IAEA, Research reactor core conversion guidebook: Volume 4: Fuels (Appendices I-K), Vienna, 1992, 594 p. IAEA-TECDOC-643 (available at https://www-pub.iaea.org/MTCD/Publications/PDF/te_643v4_prn.pdf.

[10] Joint Committee for Guides in Metrology-JCGM, Evaluation of measurement data: Guide to the expression of uncertainty in measurement, Working Group 1, Sèvres, 2008, 134 p. JCGM 100:2008 (available at https://www.bipm.org/documents/20126/2071204/JCGM_100_2008_E.pdf/cb0ef43f-baa5-11cf-3f85-4dcd86f77bd6.

[11] International Organization for Standardization-ISO. ISO/IEC Guide 98-3:2008: Uncertainty of measurement - Part 3: Guide to the expression of uncertainty in measurement (GUM:1995). 1 ed. Geneva: ISO Technical Advisory Group on Metrology (Tag 4), 2008. 120 p. (available at https://www.iso.org/standard/50461.html.

[12] International Organization for Standardization-ISO, ISO 14253-1: Geometrical product specifications (GPS) - Inspection by measurement of workpieces and measuring equipment - Part 1: Decision rules for verifying conformity or nonconformity with specifications, 3 ed., Geneva, 2017, 23 p. (available at https://www.iso.org/standard/70137.html.

[13] United Kingdom Accreditation Service-UKAS, Decision rules and statements of conformity: LAB 48, 4. ed, Middlesex, 2022, 47 p. (available at https://www.ukas.com/wp-content/uploads/schedule_uploads/759162/LAB-48-Decision-Rules-and-Statements-of-Conformity.pdf.

[14] American Society of Mechanical Engineers-ASME, ASME B89.7.3.1-2001: Guidelines for decision rules considering measurement uncertainty in determining conformance to specifications, New York, 2001, 24 p. (available at https://www.asme.org/codes-standards/find-codes-standards/b89-7-3-1-guideline-decision-rules-considering-measurement-uncertainty-determining-confirm-specifications/2001/drm-enabled-pdf.

[15] A.S. Ribeiro, M. Gölze, Decision rules applied to conformity assessment, Eurolab General Secretariat, Brussels, 2017, 14 p. Technical Report 1/2017 (available at https://eurolab-d.de/files/eurolab_technical_report_no.1-decision_rules_applied_to_conformity_assessment-2017_final.pdf.

[16] Joint Committee for Guides in Metrology-JCGM, Evaluation of measurement data: the role of measurement uncertainty in conformity assessment, Working Group 1, Sèvres, 2012. 57 p. https://www.bipm.org/documents/20126/50065304/JCGM_106_2012_E.pdf/fe9537d2-e7d7-e146-5abb-2649c3450b25.

[17] D.B. Hibbert, Quality Assurance For The Analytical Chemistry Laboratory, Oxford University Press Inc, New York, 2007, p. 321.

[18] Zaz, Ghita; Clézio, Emmanuel Le; Dekious, Ali; Alaoui, Meriem Chrifi; Calzavara, Yoann; Despaux, Gilles. In situ high-resolution measurement of HFR nuclear fuel plates' spacing. IEEE Transactions on Nuclear Science, [s.l.], v. 65, n. 11, p. 2776-2783, 11 nov. 2018. (available at https://ieeexplore.ieee.org/stamp/stamp.jsp?tp=&arnumber=8488593.

[19] Keiser Jr, D. Dennis, Walter Williams, Adam Robinson, Dan Wachs, Glenn Moore, Doug Crawford, Detailed measurements of local thickness changes for U-7Mo dispersion fuel plates with Al-3.5Si matrix after irradiation at different powers in the RERTR-9B Experiment, J. Nucl. Mater. 494 (2017) 448–460. Elsevier BV. (available at https://doi.org/10.1016/j.jnucmat.2017.07.047.

[20] M. Fabert, L. Gallais, Y. Pontillon, On-line deformation measurements of nuclear fuel rod cladding using speckle interferometry, Prog. Nucl. Energy. Amsterdam (2014) 44–48, https://doi.org/10.1016/j.pnucene.2013.10.009.

[21] Seung-kyu Park, Nak-gyu Park, Sung-hoon Baik, Young-june Kang, Visualization of internal defects in plate-type nuclear fuel by using noncontact optical interferometry, Nucl. Eng. Technol. 45 (3) (2013) 361–366. Elsevier BV. (available at https://doi.org/10.5516/net.05.2012.065.

[22] Tournant, Audrey; Magre, Frederic Alain; Loriot, Benjamin. Method for controlling the positions of nuclear fuel assemblies inside a nuclear reactor core, and corresponding control assembly. Titular: United States Patent and Trademark Office. FR n. 10.083.768 B2. Depósito: 26 jul. 2011. Concessão: 08 abr. 2013. USPTO, p. 1-7, 2018. (available at https://patentscope.wipo.int/search/en/detail.jsf?docId=WO2012022890.

[23] Joint Committee for Guides in Metrology-JCGM, Evaluation of measurement Data: Supplement 1 to the "Guide to the expression of uncertainty in measurement" - Propagation of distributions using a Monte Carlo method, Working Group 1,

Sèvres, 2008, 90 p. JCGM 101:2008 (available at https://www.bipm.org/documents/20126/2071204/JCGM_101_2008_E.pdf/325dcaad-c15a-407c-1105-8b7f322d651c.

[24] A. Coskun, W.P. Oosterhuis, Statistical distributions commonly used in measurement uncertainty in laboratory medicine, Biochemia Medica, Zagreb 30 (1) (2020) 5–17. Croatian Society for Medical Biochemistry and Laboratory Medicine. https://doi.org/10.11613/bm.2020.010101.

[25] Mitutoyo Corporation, Linear displacement sensors: Linear gage, Kanagawa: Mitutoyo Corporation (ed.), Japan, 2020, 60 p. (available at https://www.mitutoyo.com/webfoo/wp-content/uploads/E4174-572_Linear_Gage.pdf.

[26] International Organization for Standardization-ISO, ISO 1: Geometrical product specifications (GPS) - Standard reference temperature for the specification of geometrical and dimensional properties, 4 ed., Geneva, 2022, 6 p. (available at https://www.iso.org/standard/80702.html.

[27] D. Carpenter, A Further, Demystification of the U-Shaped Probability Distribution. In: International Symposium on Electromagnetic Compatibility - EMC, 2005, Chicago. Proceedings [...] . Ipswich: IEEE, 2005. p. 519-524. (available at https://ieeexplore.ieee.org/document/1513570/references#references.

[28] M.J. Puttock, E.G. Thwaite, Elastic Compression of Spheres and Cylinders at Point and Line Contact, Commonwealth Scientific and Industrial Research Organization, Melbourne, 1969, p. 64. National Standards Laboratory Technical Paper N° 25 (available at https://emtoolbox.nist.gov/publications/nationalstandardslaboratorytechnicalpaperno25.pdf.

[29] G.J.P. Nijsse, Linear Motion Systems: A modular approach for improved straightness performance. Delft University Press, 2001, 255 p. (available at https://repository.tudelft.nl/islandora/object/uuid%3Ad0ee41a2-2b65-4c7d-b54c-1cfafac63485.

[30] Japanese Industrial Standards-JIS, JIS B 7506 (JMA): Gauge blocks, Japanese Standards Association, Tokyo, 2004, 34 p. (available at https://webdesk.jsa.or.jp/books/W11M0090/index/?bunsyo_id=JIS+B+7506%3A2004.

[31] Fagor Automation (Spain) (ed.). Encoders: Linear and angular, Standard series. Mondragón, 2023. 20 p. (available at https://www.fagorautomation.com/en-us/documentation/#/.